INVESTIGATING THE EFFECTS OF A WEAK LOWER CRUST ON BASIN AND RANGE EXTENSIONAL HISTORY

by

Christopher M. Calvelage

A Thesis

Submitted to the Faculty of Purdue University

In Partial Fulfillment of the Requirements for the degree of

Master of Science

Department of Earth, Atmospheric, and Planetary Sciences

West Lafayette, Indiana

August 2021

THE PURDUE UNIVERSITY GRADUATE SCHOOL
STATEMENT OF COMMITTEE APPROVAL

Dr. Christopher Andronicos, Chair

Department of Earth, Atmospheric, and Planetary Sciences

Dr. Lucy Flesch

Department of Earth, Atmospheric, and Planetary Sciences

Dr. William Holt

Department of Geosciences, Stony Brook University

Approved by:

Dr. Daniel Cziczo

This thesis is dedicated to my parents. Thank you for believing in me.

ACKNOWLEDGMENTS

I would like to express my sincere gratitude to my thesis advisor Dr. Lucy Flesch. Her guidance has been instrumental to my growth as a scientist. This work would not have been possible without her kindness, motivation, and patience.

I thank my committee members Dr. William Holt and Dr. Chris Andronicos, their many conversations, contributions, and guidance was instrumental in fully developing this work.

I would like to thank the many fantastic professors I've had at Purdue over the years. A special thank you to Dr. Ken Ridgway, Dr. Chris Andronicos, and Dr. Saad Haq for teaching incredible classes and for fruitful discussion about this work.

I would also like to thank the National Science Foundation for funding this work. Funding for this work came from NSF#10001400.

I thank my friends Hannah Weaver, Joeseph McConoughey, Phiala Newman, Brandon Keough, Sarah Sams, Cooper Fasulo, Carlisle Wishard Allison Lafleur, Allie Jo Koester, Brayton Pew and Jack Fekete for fruitful discussion and for all the fun during my time at Purdue.

Lastly, I thank my family and my partner Gabby Buck. They have been a constant source of support and encouragement.

TABLE OF CONTENTS

LIST OF TABLES

LIST OF FIGURES

ABSTRACT

The deformation mechanisms responsible for the extension and rifting in Basin and Range extension over the past ~36 Ma, and their relative importance remain debated. Slab rollback, lithospheric body forces, and relative plate motions have all been shown to contribute, but the relative importance of each mechanism is not fully understood. Here, we build three-dimensional (3D) steady state geodynamic models to simulate the full tectonic reconstruction of Basin and Range extension and compare these results with known geologic field observations and other detailed reconstructions of surface deformation. Our modeling approximates lithospheric deformation through Stokes flow in a spherical cap of variable viscosities. By applying reconstructed boundary conditions, crustal thickness, and surface elevation at 17 Ma, and varying lithospheric viscosity we map out the predicted response of the surface motions and lower crustal flow for different assumed lithospheric viscosity contrasts and investigate the origin of core complex formation. Comparisons between predicted model deformation and geologic field observations from metamorphic core complexes and exposed fluorite deposits indicate: (1) The primary driving force of the formation of geologic features in the western US is regional gravitational collapse focused in the lower crust. Plate motions are second order by comparison at this time period and act to rotate velocities near the plate boundary. (2) A weak lower crust facilitates metamorphic core complex formation and extension in the Nevadaplano. Lateral extrusion of the lower crust serves as a mechanism for both core complex formation and the flattening of the Moho that is observed at present day. (3) Lower crustal flow is a contributes to the rotation and tilt of the Colorado Plateau and formation of the Rio Grande Rift.

CHAPTER 1. INTRODUCTION AND GENERAL OVERVIEW

Widespread extension in the western United States is recognized however, controversy remains regarding the mechanics of extension history in the Basin and Range (Flesch et al., 2000, 2007; Ghosh and Holt, 2012; Humphreys and Coblentz, 2007; Sonder and Jones, 1999). To clarify the relationships between extensional mechanisms, we propose numerical models with varying cases of lower crustal viscosity and strength partitioning to investigate the significance of differential crustal viscosities during extensional processes. Specifically, we examine the effect of a weak lower crust in the western United States as suggested by previous research (Bahadori et al; 2018; Block and Royden, 1990; Zuber et al., 1986). These numerical models provide broadly applicable insights to the importance of crustal viscosity differentials and aid in the understanding of overall motion in rifting processes around the world.

The western United States has a complex deformational history, with both thin-skinned and thick-skinned compressional deformation being overprinted by extensional tectonics and glacial processes creating modern large-scale features like the Basin and Range, Colorado Plateau and Rio Grande Rift. The Sevier and Laramide orogenies created large orogenic plateaus with thick crustal roots, most notably the Nevadaplano, Mogollon Highlands, and the Rocky Mountain foreland (Dickinson et al, 2002, 2006). Following this compressional tectonic regime, western North America experiences a dramatic shift to an extensional tectonic regime during the Eocene. At approximately 40 Ma the region underwent a transition from shallow to flat slab subduction to the current transtensional regime with the initiation of the San Andreas fault (Dickinson, 2006). This transition destabilized the acting stress field and began altering high plateau elevations to the modern Basin and Range topography (McQuarrie and Wernicke, 2005)

Current research estimates ~200% east-west extension in the southernmost portion of the Basin and Range and ~50% in the northern regions (McQuarrie and Wernicke, 2005). Extension of these magnitudes produces regions of exposed deep crustal metamorphic rocks called metamorphic core complexes (Davis et al. 1980). During extensional processes, as the crust thins, deep crustal strata are exhumed from beneath an area of detachment and are exposed at the surface (Davis et al, 1980; Wernicke and Axen, 1988). Metamorphic core complexes are characterized by

a core of high-grade metamorphic rocks, large vertical uplift, and a cap of highly sheared, attenuated, and variably metamorphosed sedimentary rock. The formation of these structures remains controversial. Mechanisms include; extension on low angle normal faults (Wernicke, 1981), intrusions of plutons (Lister and Baldwin, 1993), the rotation of high angle normal faults (Buck, 1988), and the extrusion of a weak lower crust (Wernicke et al, 1992; Martinez et al., 2001). It is widely accepted that these features are unique to extensional regions and are abundant in the Basin and Range. These core complexes record shear vergence direction and can be used as a proxy for the direction of lower crustal flow during formation (Wernicke, 1981). Extension of these magnitudes also produces magmatism. Fluorite deposits genetically related to alkalic magmatic deposits can be used as a proxy for subsidence. As the crust is attenuated, fluorite rich deposits are exhumed (Lamarre and Hodder, 1978). These two geologic data are used for model validation.

Large-scale geologic features like the Colorado Plateau and Rio Grande Rift also contribute to the deformational signature in the Western U.S. Though its deformational history is debated, the Colorado Plateau is thought to be a coherent crustal domain that has undergone uplift with very little internal deformation (Roy et al., 2009; Bird 1979). Despite undergoing little deformation, the plateau itself plays a role in the opening of the Rio Grande Rift (Chapin and Cather, 1994). Previous studies have linked a rotation of 1.0-1.5 degrees of the Colorado Plateau about an Euler pole near the Utah-Wyoming border to the extensional behavior of the Rio Grande Rift (Chapin and Cather, 1994). The Rio Grande Rift has undergone 8-12% extension in the North and up to 50% in the southern portion on the rift (Chapin and Cather, 1994; Aldrich et al., 1986; Morgan et al., 1986). We will use these proposed deformational behaviors to compare our calculated model outputs as a form of model verification.

Though the mechanics of modern Basin and Range extension are well understood, controversy remains regarding what driving mechanisms are responsible for past Basin and Range extension. Slab rollback, lithospheric body forces, and plate boundary conditions all contribute, but the relative importance of each mechanism is not understood as the Basin and Range evolved (Flesch et al., 2000, 2007; Humphreys and Coblentz, 2007; Ghosh and Holt, 2012). A complete understanding of these mechanisms of deformation requires a model that incorporates interactions

with the mantle and lithosphere but also the influence of gravitational collapse from lithospheric body forces. The Basin and Range presents a unique opportunity to study these mechanisms due to the comprehensive reconstructions of extension (Coney and Harms, 1984; McQuarrie and Wernicke, 2005), density, viscosity, crustal thickness (Bahadori et al, 2018; Bahadori and Holt, 2019), and geologic constraints (i.e. metamorphic core complexes and fluorite deposits) (Dickenson, 2002; Lamarre and Hodder, 1978). Bahadori et al (2018) reconstruct the crustal thickness and paleotopography of the Basin and Range to 36 Ma. They show thick crustal roots underneath regions of orogenic plateaus. Because the modern Moho is flat below regions of metamorphic core complexes (Snow and Wernicke, 2000), we suggest that the paleo-root was flattened as lower crustal rocks were exhumed. This indicates a weak lower crust facilitating the extension of paleo-roots and paleo-topography prior to- and during extension in the Western United States (Bahadori et al. 2018). This study will implement a full 3D finite element model with reconstructed viscosity, density, crustal thickness and a weak lower crust. We will use these models to systematically examine the effects of differing viscosity structures on the regional extensional tectonics of the western U.S. and the formation of metamorphic core complexes. We present the results from a suite of viscosity parameter variations and discuss the fit of deformation with known geological observations.

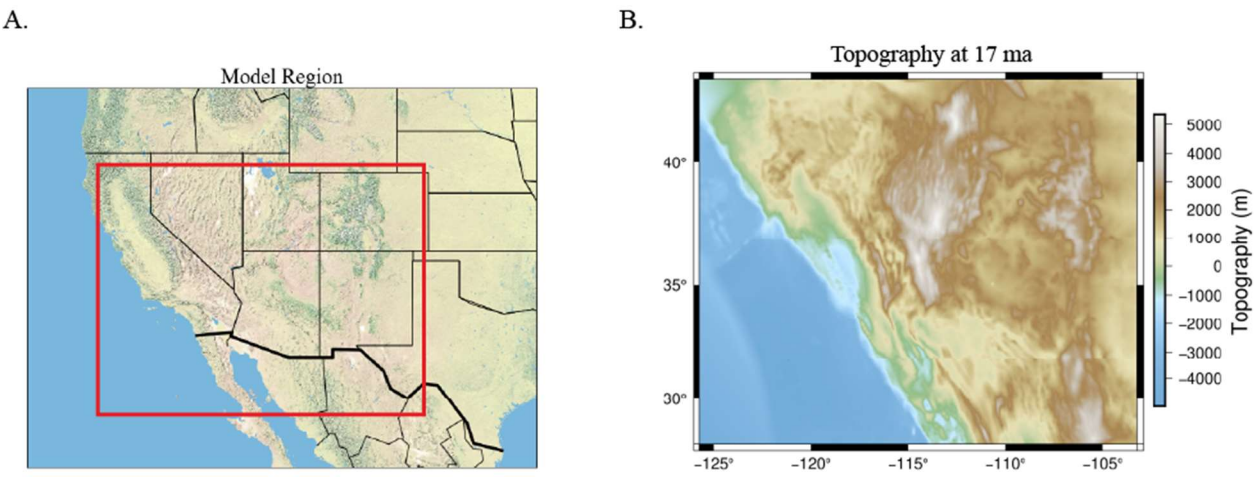

Figure 1: A) Modern topography of the western United States with the model region denoted by the red rectangle. B) Topography of the model region at 17 Ma; the time-step of interest (Bahadori et al, 2018).

CHAPTER 2. METHODS

2.1 Physics

We use COMSOL Multiphysics (www.comsol.com) finite element modeling software to construct the model geometry, input the material properties and boundary conditions, mesh the geometry, and solve the Stokes flow equations. We perform our computations at the 17 Ma time step. This time-step allows for a detailed analysis of the imminent collapse of the Nevadaplano and deformation of the Moho in conjunction with comparisons with active metamorphic core complexes and fluorite deposits.

Following methods from Bischoff and Flesch (2018, 2019) we assume that deformation of the lithosphere is expressed as flow of an incompressible Newtonian fluid governed by the equations for Stokes flow:

$$-\eta(x,y,z)\nabla^2\mathbf{u}(x,y,z) + \nabla p(x,y,z) = \mathbf{F}(x,y,z)$$

$$\nabla\bullet\mathbf{u}(x,y,z) = 0$$

where η is viscosity, $\mathbf{u}$ is fluid velocity, p is pressure, and $\mathbf{F}$ represents body forces generated by gravitational potential energy. for each finite element, η represents the depth-dependent laterally varying viscosity value and $\nabla p(x,y,z)$ represents the pressure forces, which inherently include forces arising from density variations and applied boundary conditions. Gravity acting upon each finite element is accounted for within the body forces. We then solve this equation for the displacement vector field $\mathbf{u}(x,y,z)$ of each finite element.

2.2 Model Geometry

In order to utilize and compare with previous 2D results from Bahadori et al (2018) the model region of the western United States extends westward from -104° to -123°, northward from 28° to 43°, and vertically downward to 100 km below sea level. This creates a 3D spherical cap

that represents the lithosphere of the western U.S. We choose a vertical depth of 100 km to remain consistent with vertical averages of viscosity from Bahadori et al (2018) that we use in the modeling. Additionally, as supported by similar 3-D geodynamic models of the Indian-Eurasian collision zone (Bischoff & Flesch, 2018, 2019), not extending our model below 100 km excludes forces arising from dynamic topography, which are not included in the force balance equations for these simulations. We partition the geometry using the reconstructions of both paleotopography and crustal thickness from Bahadori et al (2018). The lower crust is assumed to begin at 20 km depth to account for the brittle-ductile transition, the beginning of the mid and lower crust (Benz et al., 1990), and create a domain for finer control of mesh density. We also partition and remove a domain that roughly consists of the oceanic crust; where there is no longer lower crust and where lower crustal domain becomes too thin for adequate meshing (Figure 2, 3). This does not impact model results because the boundary conditions still contain the slight motion from the pacific plate that is transmitted to the continent (Figure 4C).

We optimize mesh discretization by comparing solutions with various mesh densities. We select the lowest mesh density that still gives comparable results with higher density meshes. Our optimal mesh contains 301,725 mesh elements with the largest element being 172 km in the oceanic domain of the model. Meshing is performed after the creation of the model geometry so mesh elements respect the internal boundaries of the geometry.

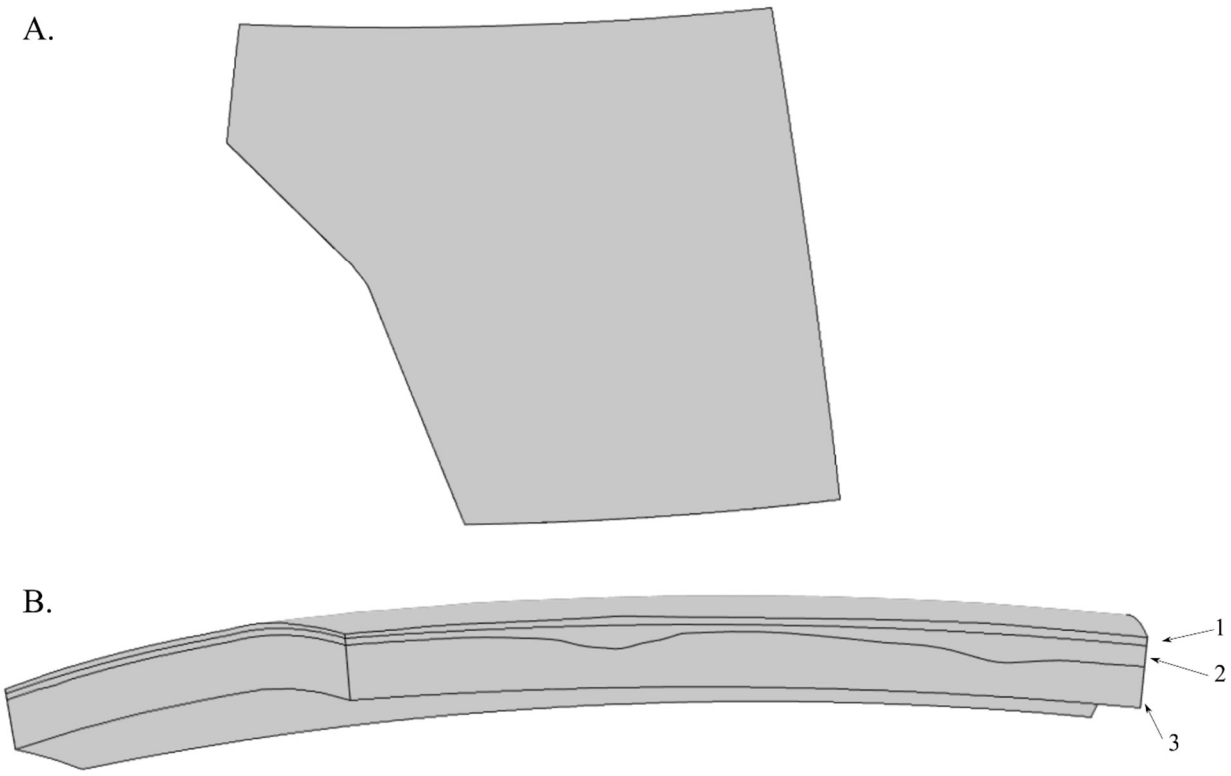

Figure 2: The 3D model geometry of the model region. A) Model region from above. B) A side view of the model geometry showing the different model domains. 1, 2, 3 are the upper crust, lower crust, and lithospheric mantle respectively.

A.

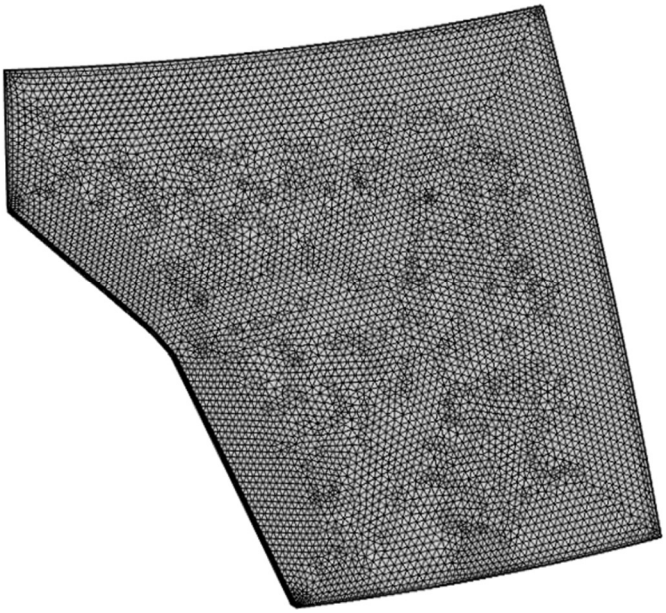

B.

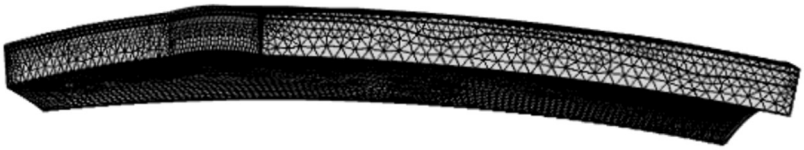

Figure 3: The 3d mesh solution for our model geometry. A) Model region mesh from above. B) A side view of the model geometry showing the different model domains. Domains remain the same as in Figure 2.

2.3 Boundary Conditions

We use velocity boundary conditions from Bahadori and Holt (2019) (Figure 4A) and interpolate the input boundary conditions over the model geometry region and apply the interpolation along the vertical model sidewalls. We only use velocity conditions on the continent to avoid subduction effects. The resulting boundary conditions represent only motions within the continent and excludes the modeling the subduction region where the assumption of incompressible flow breaks down (Figure 4B, C). We apply a stress-free boundary condition on the model surface to approximate surface-atmosphere interactions as a zero stress. We apply a volume body force to every model domain to approximate the effect of gravity. Lastly, we apply a free slip condition at the base of our 3-D volume and assume that mantle tractions are not a major driving force.

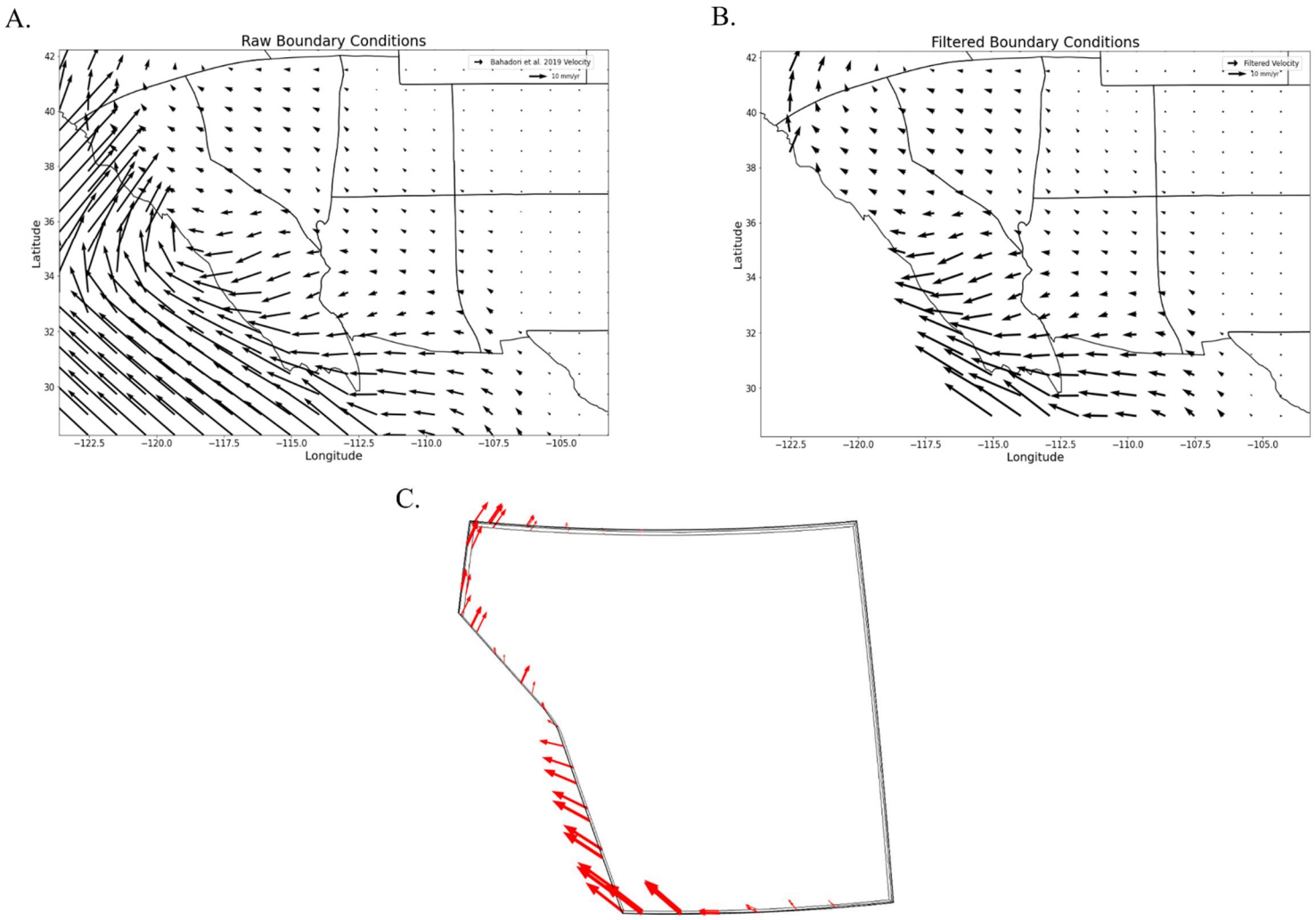

Figure 4: A) Full surface velocities calculated by Bahadori and Holt. (2019) B) The same velocity field fit to the model geometry. C) The 3D boundary conditions applied to the full model geometry.

2.4 Material Properties

2.4.1 Density

We use 3D density data for the lithospheric mantle from Bahadori and Holt (2019) and assume a crustal density of 2830 kg/m^3. We calculate the vertically and laterally varying value at each location within the model. This data is interpolated into a data cube with a depth increment of 0.5 km and a lateral resolution 0.5° (Figure 5).

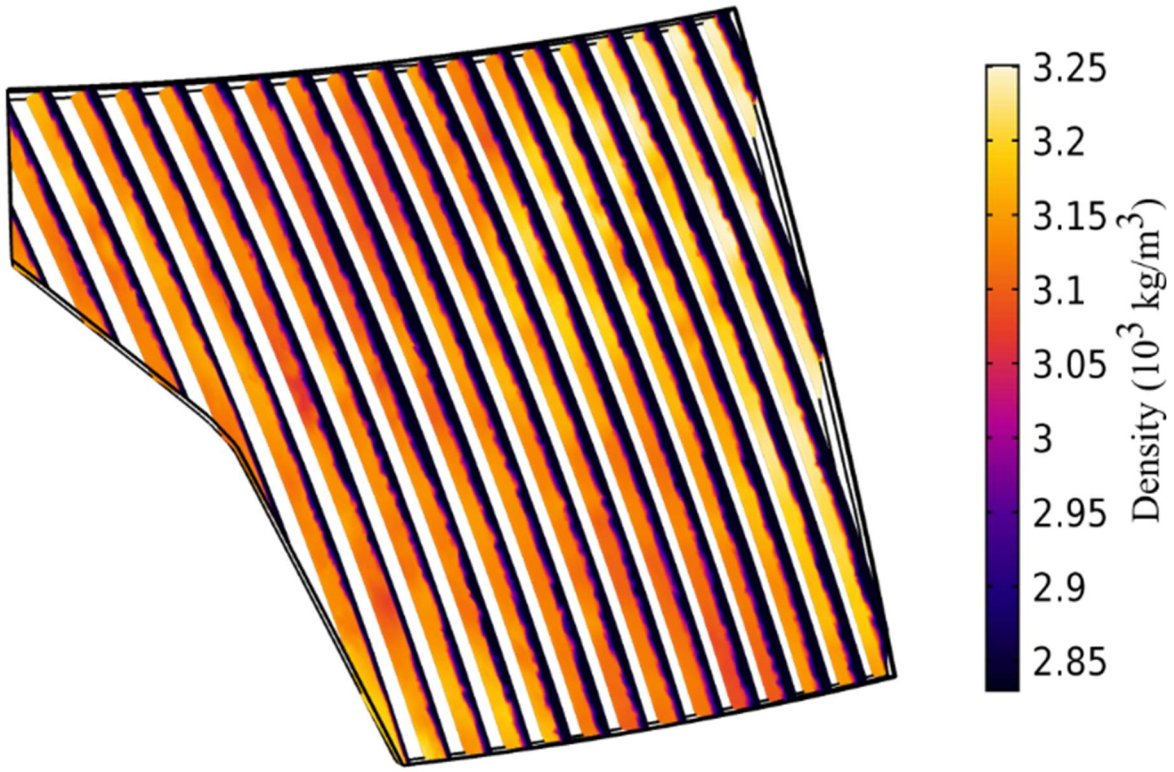

Figure 5: 3D density slices through the model region. Upper and lower crustal density is assumed to be 2830 kg/m3 and the lithospheric mantle densities are from Bahadori and Holt (2019) and interpolated to fit the model geometry.

2.4.2 Viscosity

We use the vertically average effective viscosity from Bahadori and Holt (2019) (Figure 6A) as a constraint that all assumed 3-D viscosity distribution must all match. We assume a crustal and mantle viscosity in the 3D model geometry using the following relationship:

$$t_T\ \eta_T = t_M\ \eta_M + t_{LC}\ \eta_{LC} + t_{UC}\ \eta_{UC}$$

where t_T, t_M, t_{LC}, and t_{UC} are lithospheric, lithospheric mantle, lower crustal, and upper crustal thickness, respectively; η_T, η_M, η_{LC}, and η_{UC} are vertically averaged, lithospheric mantle, lower crustal, and upper crustal viscosities. After Partitioning the viscosities according to the above equation, we input a 3D viscosity profile into the model (Figure 6B). We use constant lower crustal viscosities of 10^{20} and 10^{19} Pa-s for η_{LC} in combination with different partitions of upper crustal strength to lithospheric mantle strength (FCM). For example, an FCM of 1 means that the upper crust and lithospheric mantle have the same strength and an FCM of 5 would mean that the upper crust is 5 times stronger than the lithospheric mantle. To cover a range of crustal viscosity structures we choose FCM ratios of 1, 5, and 10.

A.

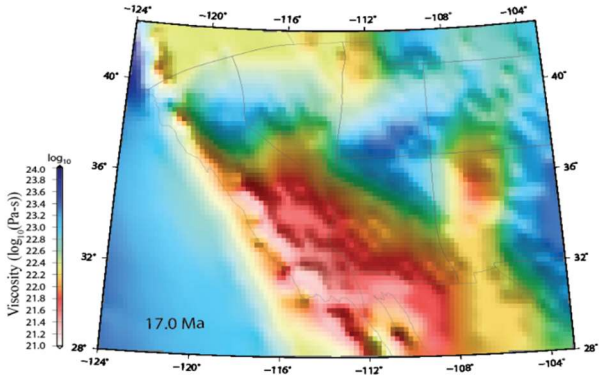

B.

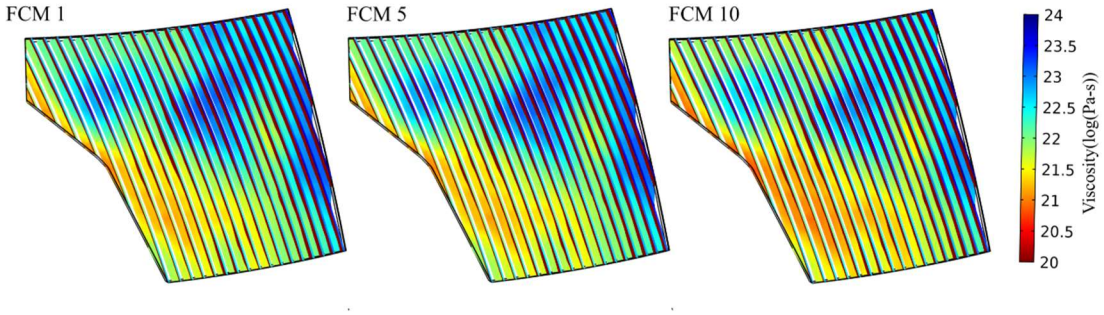

Figure 6: A) Vertically averaged viscosity at 17 Ma from Bahadori and Holt (2019). B) Partitioned 3D viscosity profiles for FCM cases 1, 5, and 10.

2.5 Geologic Data

We use geological observations in the form of metamorphic core complex locations (Bahadori et al., 2018) and mapped vergence directions (Dickinson, 2002) (Table 1) and exposed fluorite deposits (Lamarre and Hodder, 1978) (Figure 7). We assume that the vergence directions measured in the metamorphic core complexes corresponds to the direction of lower crustal flow at the time of recording and that the fluorite deposits are exposed due to subsidence during extension. This allows for comparison of model outputs to the known geological constraints to reduce non-uniqueness in the numerical solutions.

Table 1: A list of the active metamorphic core complexes and their vergence directions at 17 Ma. Reconstructed core complex locations are from Bahadori et al. (2018) and their vergence directions are from Dickinson (2002).

Name	**Longitude**	**Latitude**	**Inferred vergence direction (Degrees)**
Sacramento	-115	35	56
Harcuvar	-113.02	33.9	53.0
Harquahalla	-112.7	33.8	53.0
Buckskin	-113.37	34.16	37.2
Whipple	-114.17	34.3	43.4
Chemehuevi	-114.48	34.55	49.9

CHAPTER 3. RESULTS

Currently, lateral variations of viscosity in the Basin and Range lithosphere are well understood, however, the vertical distribution of lithospheric strength remains contested (Burov & Watts, 2006; Jackson, 2002). Two main frameworks have come to the forefront of the debate: Jackson (2002) argues that the frequency of earthquakes occurring in the upper crust is most easily explained if most of the lithospheric strength concentrated there, proposing the "crème- -brûlée" model of the lithosphere where the crust is strong and brittle and the mantle is weak and ductile. Conversely, earthquake focal depth observations posed by Chen and Molnar (1983) and laboratory experiments on rock strength, temperature, and pressure conducted by Kohlstedt et al. (1995) indicate that strength could be partitioned in the upper crust and lithospheric mantle surrounding a weak lower crust, proposing the "jelly sandwich" model of the lithosphere. Burov and Watts (2006) created a suite of 2D thermomechanical models that showed the "crème- -brûlée" model was unable to support mountain ranges over 10 million year, arguing in favor of the "jelly-sandwich" model. Thus, in order to constrain the vertical viscosity strength partitions for the western U.S. we use a suite of different viscosity combinations and quantitatively compared to the horizontal surface velocity model reconstructions of Bahadori and Holt (2019).

We use the topography, crustal thickness, density, viscosity, and velocity conditions at 17.0 Ma from Bahadori et al (2018) and Bahadori and Holt (2019) to solve the Navier-Stokes equations producing an instantaneous velocity and stress solution that is consistent with known geologic observations. We compare solutions with a lower crustal viscosity of 10^{19} and FCM cases of 1, 5, and 10 to models with a lower crustal viscosity of 10^{20} with FCM cases 1, 5, and 10 by calculating the RMS misfit between model predicted surface velocities and reconstructed surface velocities. Lastly, we compare our preferred model of FCM 5 with a lower crustal viscosity of $10^{20.3}$ and a model containing the same parameters with fixed boundary conditions to inform the influence of gravitational collapse on Basin and Range extension.

3.1 Surface velocity comparison and preferred model selection

Predicted velocities at the surface of the model are quantitatively compared to the horizontal surface velocity model reconstructions of Bahadori and Holt (2019) (Table 2) and model predicted vertical velocity signatures are compared to exposed fluorite deposits (Lamarre and Hodder, 1978) to map out the best-fit viscosity contrast between the upper crust and lithospheric mantle.

3.1.1 Models with a lower crustal viscosity of 10^{19}

For each FCM case with a lower crustal viscosity of 10^{19} Pa-s we implement the geometry discussed above (Section 2.2) (Figure 2), a 3D partitioned density (Figure 5), and the reconstructed boundary conditions fit to the model geometry applied to all model sidewalls (Figure 4). We apply a body force on the entire model domain to simulate the effect of gravity. Lastly, we implement differing partitions of upper crustal to lithospheric mantle strength for FCM 1, 5, and 10.

FCM 1

For this simulation we use a FCM value of 1, meaning that the upper crust and the lithospheric mantle have the same value and surround a weak lower crust. Overall, the predicted velocities are poor fit (Table 2) with the reconstructed velocities. In particular, the region surrounding the Nevadaplano has very large misfit. Horizontal velocity magnitudes are vastly overpredicted and their vergence directions display considerably more southward rotation than the reconstruction (Figure 7A). The large misfit here is likely due to the increased effect of gravity on the relatively weaker upper crust. This allows for more material to be pushed southward from the high topography of the Nevadaplano and does not allow for the northward rotation associated with the Pacific plate as the boundary conditions are not transferred inboard through a weak upper crust. Vertical velocities for this simulation are unrealistically high, with subsidence rates of up to 50 mm/yr (Figure 7A). Though vertical magnitudes are unrealistically large, it should be noted that the general pattern of subsidence fits well with fluorite deposit data. Maximum rates of subsidence are generally co-located with fluorite locations.

FCM 5

Having an increased upper crustal viscosity provided an improved fit with the reconstructed velocities (Table 2). Here we see a much weaker influence from gravity, a stronger rotation towards the imposed boundary condition vergence direction, and reduced velocity vector magnitudes throughout the entire model domain (Figure 7B). Vectors in the Nevadaplano still exhibit more southward rotation due to the larger contribution from GPE associated with the high topography. As expected, the vertical velocity magnitudes are still physically unrealistic. Subsidence rates reach maximums of 50 mm/yr, and maintain a matching pattern with fluorite deposit locations.

FCM 10

For this simulation we increase the upper crustal strength to a FCM of 10, meaning the upper crust is an order of magnitude stronger than the lithospheric mantle. Like the FCM 5 case this simulation has an improved fit with the reconstructed velocities (Table 2). The differences in both horizontal velocities and vertical velocities between this case and the FCM 5 case are nearly imperceptible (Figure 7C). Vertical velocities for this model continue to have magnitudes of up to 50 mm/yr. We interpret this to mean that after FCM 5 the strength of the upper crust plays a small part in the deformational signature and that the vertical velocities produced by these simulations are largely controlled by the viscosity value used for the lower crust.

3.1.2 Models with a lower crustal viscosity of 10^{20}

For each FCM case with a lower crustal viscosity of 10^{20} Pa-s we implement the geometry discussed above (Section 2.2) (Figure 2), a 3D partitioned density (Figure 5), and the reconstructed boundary conditions fit to the model geometry applied to all model sidewalls (Figure 4). We apply a body force on the entire model domain to simulate the effect of gravity. Lastly, we implement differing partitions of upper crustal to lithospheric mantle strength for FCM 1, 5, and 10.

FCM 1

We begin with the FCM 1 case as we did above. Much like the FCM1 case with a lower crustal viscosity of 10^{19} Pa-s this case also shows the predicted velocities poorly fit (Table 2) with

the reconstructed velocities. Again, the region surrounding the Nevadaplano has the largest misfit. Horizontal velocity magnitudes are vastly overpredicted and their vergence directions display considerably more southward rotation than the reconstruction (Figure 8A). The large misfit here is likely due to the increased effect of gravity on the high topography with a relatively weaker upper crust. This allows for more material to be pushed southward from the high topography of the Nevadaplano and does not allow for the northward rotation supplied by the boundary conditions. Though this case has the highest RMS misfit among 10^{20} Pa-s cases, it is improved from the previous suite of 10^{19} cases. Vertical velocities magnitudes have also improved. Maximum subsidence rates of up to 10 mm/yr are colocated with high topography across the model region (i.e., Nevadaplano, Rocky Mountains, Rio Grande rift). The subsidence pattern in this case matches well with fluorite locations. We interpret the changes in vertical velocity rates to be due to the increased lower crustal viscosity, which is better able to support topography.

FCM 5

Increasing the FCM to 5 improves the misfit between predicted velocities and reconstructed velocities for this case (Table 2). Horizontal velocity magnitudes now fit well with reconstructed velocities. The orientation of these vectors is also improved throughout most of the model domain. In regions of highest topography, like the Nevadaplano, vector orientations remain rotated southward (Figure 8B). Vertical velocity signatures look nearly identical to the previous FCM case. Again, maximum subsidence rates of up to 10 mm/yr are colocated with the Nevadaplano, Rocky Maintains, and Rio Grande rift. The subsidence pattern continues to have a good fit with fluorite deposit locations.

FCM 10

Like the FCM 5 case this simulation has an improved fit with the reconstructed velocities (Table 2). The differences in both horizontal velocities and vertical velocities between this case and the FCM 5 case are nearly imperceptible (Figure 8C). Vertical velocities for this model continue to have magnitudes of up to 10 mm/yr. We interpret this to mean that after FCM 5 the strength of the upper crust plays a small part in the deformational signature and that the vertical

velocities produced by these simulations are largely controlled by the viscosity value used for the lower crust.

3.1.3 Model parameter variation summary

It is clear that the inclusion of a thickened weak lower crust impacts the surface velocity field and vertical velocity magnitude. Vector orientations in the Nevadaplano (latitude 34-36) trend more Southwest, indicating a stronger gravitational potential energy (GPE) signal as high topography collapses. Moving toward the Pacific, these velocities rotate to become plate parallel. North Western regions of the model have a vector field oriented North-Northeast. These trends are evident in every combination of model parameters.

We compare 3D model predicted surface velocities with those calculated by Bahadori and Holt. (2019) (Figure 7). Models containing a lower crustal viscosity of 10^{19} were initially considered because of a good fit with horizontal surface velocities from Bahadori and Holt. (2019) but were ruled out because they produce vertical velocities that are unrealistic (Figure 7A, B, C). RMS misfit and model predicted vertical velocities show FCM cases 5 and 10 with a lower crustal viscosity of 10^{20} as being the most robust combinations of material properties. We choose FCM 5 as our best fit model due to the lowest RMS misfit and produces realistic vertical velocities.

Table 2:A table containing all the FCM case variations and the calculated RMS misfit. We calculate the RMS misfit as in Holt et al. (2000).

Lower Crustal Viscosity Value	**Boundary Condition**	**FCM Case**	**RMS Misfit (mm/yr)**
19	Active	1	3.4877
19	Active	5	1.4327
19	Active	10	1.4250
20	Active	1	2.0827
20	Active	5	1.3108
20	Active	10	1.3148
20.3	Active	5	1.3150
20.3	Fixed (Gravity only)	5	4.5856

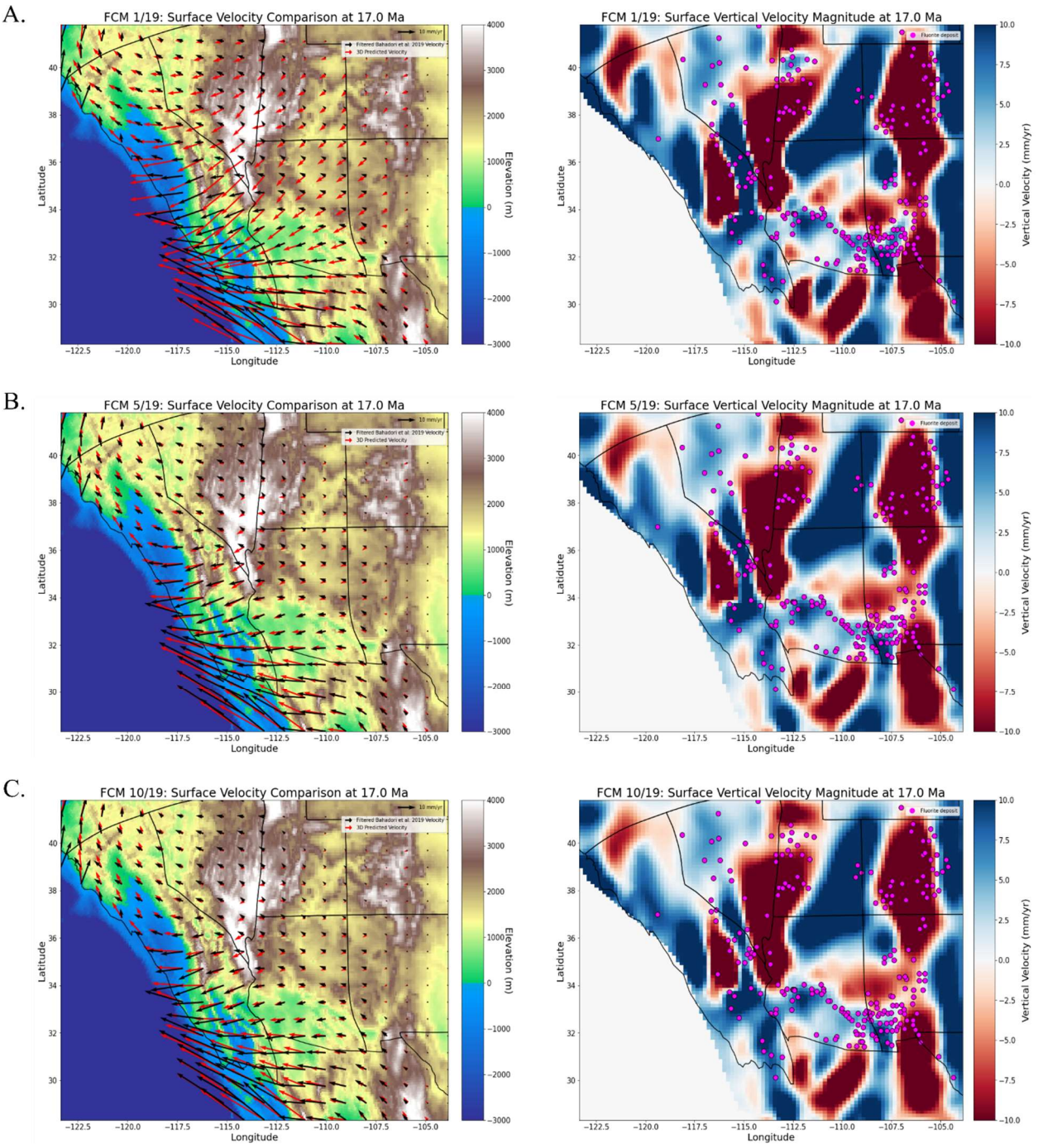

Figure 7: A, B, and C are model predicted surface velocities (red) and surface velocities produced from Bahadori and Holt (2019) (black) for models with a lower crustal viscosity of 10^{19} Pa-s. Fluorite deposits (Lamarre and Hodder, 1978) are denoted by magenta dots

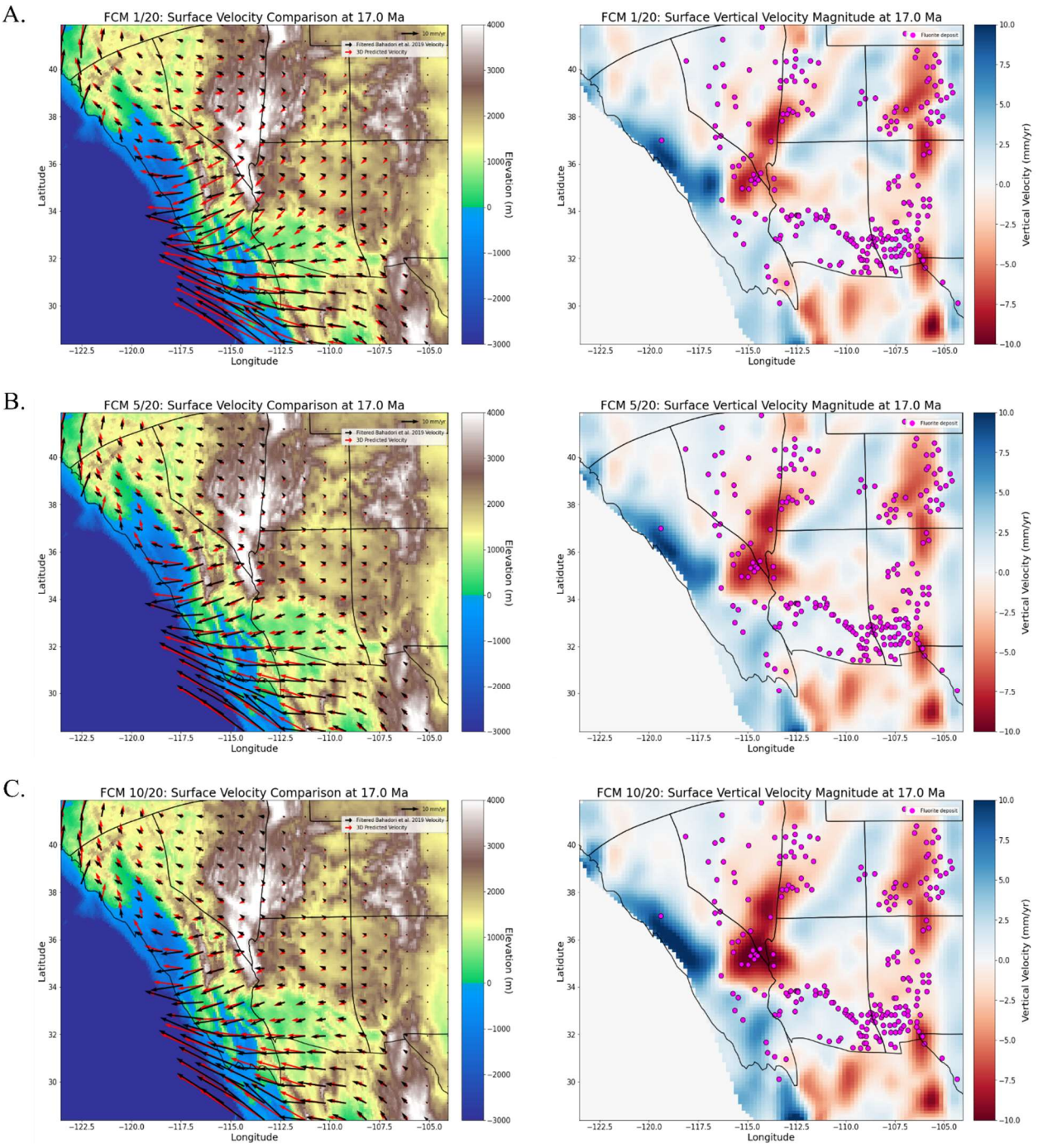

Figure 8: A, B, and C are model predicted surface velocities (red) and surface velocities produced from Bahadori and Holt (2019) (black) for models with a lower crustal viscosity of 10^{20} Pa-s. Fluorite deposits (Lamarre and Hodder, 1978) are denoted by magenta dot

3.2 Best-fit model

After observing the sensitivity of the vertical velocity magnitude to the magnitude of lower crustal viscosity we modified the FCM 5 case to incorporate a slightly stronger lower crust of $10^{20.3}$ to further decrease the vertical velocity magnitude. All other parameters remain the same as the previous cases. We compare this best fit model with reconstructed surface velocities, fluorite deposit locations, metamorphic core complex location and vergence, and a "gravity only" fixed boundary model.

With this adjustment the RMS misfit stays at 1.31 mm/yr and the vertical velocity magnitude in regions of subsidence have a maximum of 5.5 mm/yr, (Figure 11A). As in previous cases, the model predicted horizontal velocities trend more southwest than the reconstructed velocity field from Bahadori and Holt. (2019) (Figure 9) in the Nevadaplano. This simulation produced several regions of high lower crustal flow. The Nevadaplano, Rocky Mountain, and Rio Grande rift all experience high magnitude of lower crustal flow. In the southern Nevadaplano velocities in the lower crust trend southwest while velocities in the northern Nevadaplano trend East-West around latitudes 38-40 and longitude -115 and southeast around latitude 36 and longitude -112.5. This change in lower crustal flow direction from south to north along the Nevadaplano is likely due to the change in orientation of the highest topography along the plateau. This case also produces lower crustal flow in the Rocky Mountains that trends East- West at latitudes 38-40 and southeast into the Colorado Plateau at latitude 36. Lastly, the Rio Grande rift also exhibits high magnitudes of lower crustal flow. Here, vectors trend largely East-West along a North-South rift axis. Magnitudes of flow decrease moving northward as crustal thickness decreases (Bahadori et al., 2018) and the proposed Euler pole is approached (Chapin and Cather, 1994). We expect differences in surface vector rotation because the tectonic model of Bahadori and Holt (2019) assumes that the vertical variation of horizontal velocities within the lithosphere is small in comparison with horizontal gradients of horizontal velocities. Therefore, their tectonic model does not account for vertical displacements associated with lower crustal flow, and viscosity variations within the lithosphere. Differences between the two models highlight the importance and influence of a weak lower crust.

Vertical velocity magnitudes have been drastically reduced in this case compared to those with a lower crustal viscosity of 10^{19} Pa-s. Maximum subsidence rates reach 5.5 mm/yr in the Nevadaplano and 1,5-3.5 mm/yr from the Rio Grande rift north to the Rocky Mountains. Parts of the Colorado Plateau also experience very small magnitudes of uplift ranging from 0-0.5 mm/yr and subsidence ranging from 0-0.5 mm/yr. Because the pattern expressed in vertical velocity signatures is nearly identical for each model case, we interpret the primary driver to be gravitational potential energy with the lower crustal viscosity only modifying the magnitude of vertical velocity for each case, irrespective of the FCM used.

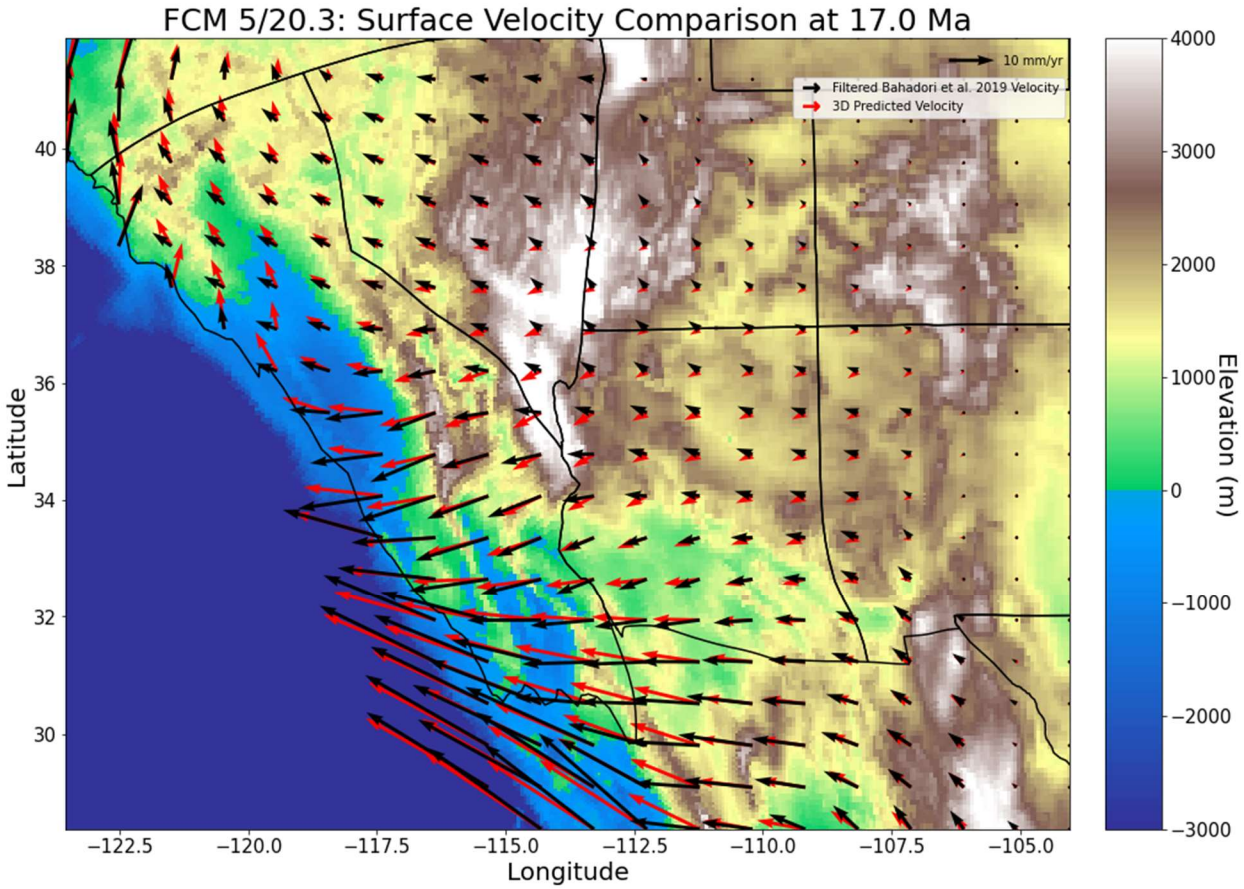

Figure 9: Best fit model predicted surface velocities (red arrows) plotted with the reconstructed velocities from Bahadori and Holt (2019) (black arrows).

3.2.1 Best fit model comparison with geologic constraints

We examine the relationships between model predicted surface velocities and lower crustal velocities and metamorphic core complex data (Figures 10 and 11); as well as model predicted vertical velocities and exposed fluorite deposits. Metamorphic core complexes active at 17 Ma have vergence directions ranging from 37-56 degrees (Table 1) from North, indicating that the model predicted lower crustal velocity field should have similar vergence in the Nevadaplano region. When compared the lower crustal velocity field does match well with measured metamorphic core complex vergences. This indicates the flow of the lower crust coincides with what was recorded during metamorphic core complex formation and that gravitational collapse is the driver. In the horizontal velocities the increased strength portioned in the upper crust allows for increased boundary condition influence while the gravitational potential energy primarily effects the lower crust. This model case also has a good fit with the locations of exposed fluorite deposits. Regions of model predicted subsidence follow the same general pattern expressed in the fluorite data indicating the model produces an accurate representation of gravitational potential energy distribution.

3.2.2 Best fit model comparison with a fixed boundary case

To understand the complex relationship between boundary conditions and gravitational potential energy on extensional deformation in the Basin and Range we also compare the preferred model to one where we use the same interior parameters and fix the vertical side boundary conditions to be fixed turning off plate motions and assessing the effects on the predicted deformation as a response to gravity only (Figure 10, 11). Interestingly, these solutions produce very similar results in interior of the model domain. Regions like the Colorado Plateau, Rocky Mountains, and Rio Grande Rift remain largely unchanged between the two solutions. As expected, the solutions begin to differ closer to the plate boundary starting near the Nevadaplano. The fixed boundary condition case produces more heavily Southward-oriented velocity vectors, and the fit between metamorphic core complex vergence directions is not as robust as the best fit model that incorporates plate motions. Vertical velocities between the two solutions are nearly identical with the fixed case only have slightly higher magnitudes at 6 mm/yr. We interpret this to show that gravitational potential energy acting on the weak lower crust is responsible for

generating the vertical velocity magnitudes while the plate boundary conditions act to rotate vectors horizontal velocities near the plate boundary.

A.

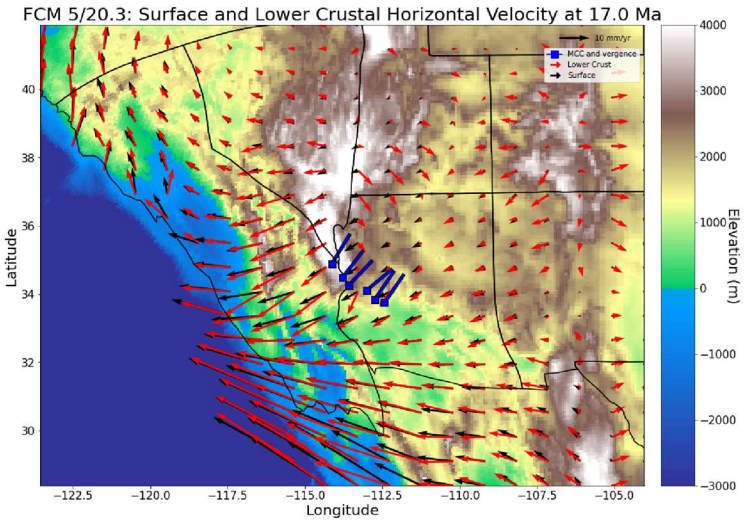

B.

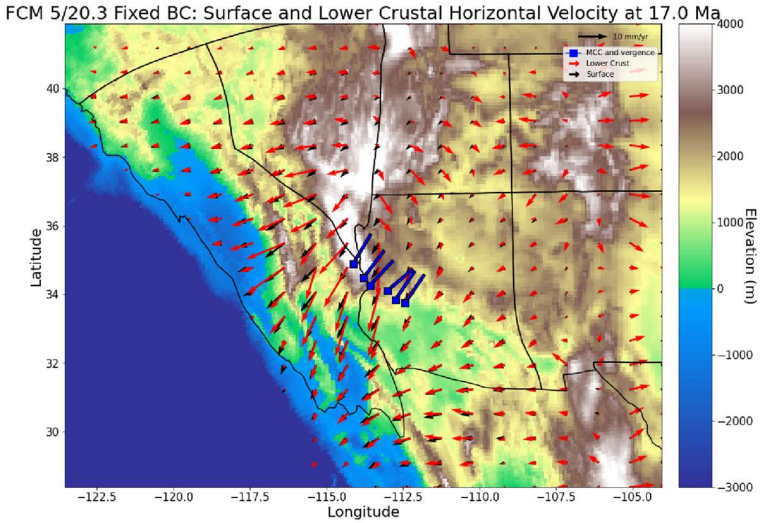

Figure 10: A) Model predicted surface and lower crust velocity solutions, metamorphic core complex locations and vergence direction for FCM case 5 with a lower crustal viscosity of $10^{20.3}$ and active boundary conditions. B) same as A but with fixed boundary conditions so the acting force is gravitational collapse. For both A and B surface velocity is indicated by black arrows, lower crustal velocity is indicated my red arrows and metamorphic core complex locations and vergence directions (Dickinson, 2002) are indicated by blue squares with tick marks.

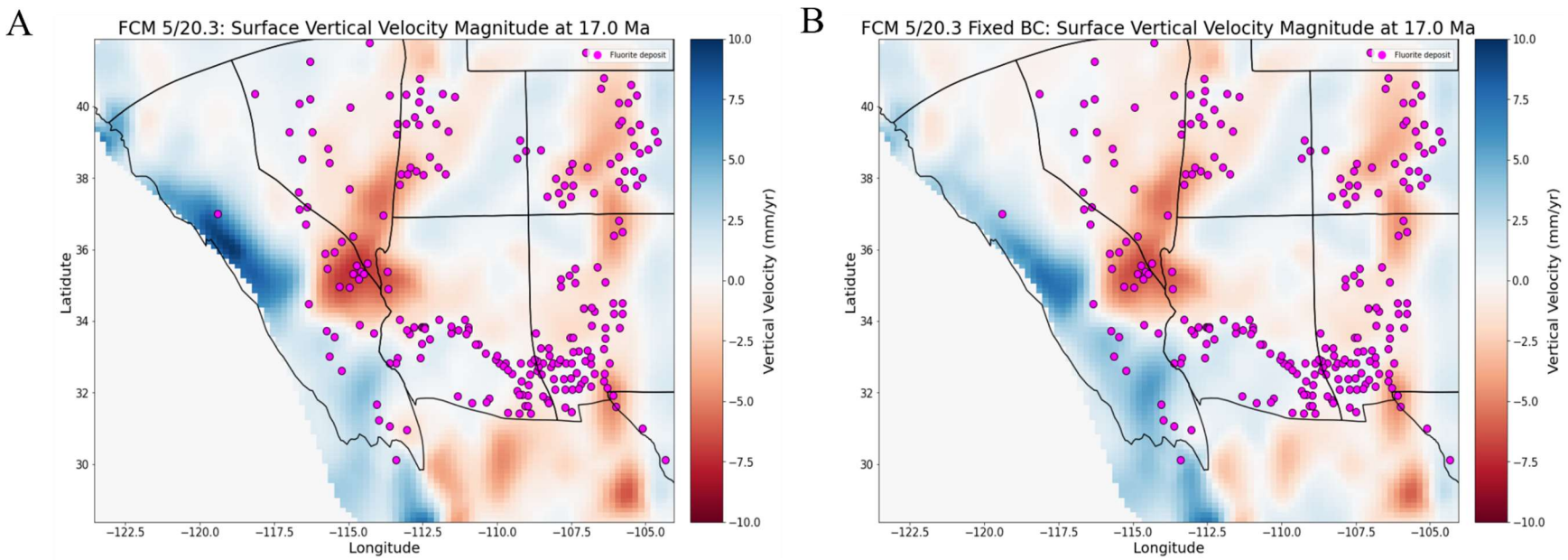

Figure 11: A) Model predicted vertical velocity solutions with exposed fluorite deposits (magenta dots) (Lamarre and Hodder, 1978) for FCM case 5 with a lower crustal viscosity of $10^{20.3}$ and active boundary conditions. B) same as A but with fixed boundary conditions so the acting force is gravitational collapse.

3.3 Best fit model cross-section description

A benefit of modeling in three dimensions is that it allows for a detailed internal look at areas of interest. We choose three cross sections: two from southwest to northeast and one from northwest to southeast (Figure 12). These allow for velocity information at depth in the Nevadaplano, Colorado Plateau, Rocky Mountains, and Rio Grande Rift.

3.3.1 A – A'

This cross-section cuts through the Nevadaplano, Colorado Plateau, and Rocky Mountains. It should be noted this is parallel to the metamorphic core complex vergence directions. In the Nevadaplano a strong lower crustal velocity signal exists with magnitudes of up to 25 mm/yr. It appears most of the motion occurs in the lower crust the vectors in this region indicate highest rates of subsidence (as shown in Figure 11A) and a southwest extensional direction. Conversely, the Colorado Plateau exhibits little to no motion and is not influenced by the deformation occurring in the part of the Nevadaplano. Lastly, the Rocky Mountains exhibit some collapse, though it is small compared to the Nevadaplano. Magnitudes of motion in the Rocky Mountains are smaller towards the Colorado Plateau, likely due to its higher viscosity.

3.3.2 B – B'

This cross-section exhibits many of the same characteristics as the previous one. Again, the largest motion in the Nevadaplano is in the lower crust with magnitudes of up to 25 mm/yr. This region also experiences similar subsidence rates as above. The Colorado Plateau continues to exhibit little deformation. In the Rocky Mountains the same signal of collapse is visible with flow occurring in the lower crust on either side of the topographic axis.

3.3.3 C – C'

This northwest-southeast cross-section exhibits many of the same features as the previous sections, but provides a deeper look across the upper Nevadaplano and the Rio Grande Rift. In the northern portion of the Nevadaplano the magnitudes of flow are lower, but largely still occurring in the lower crust. An interesting difference between this cross section and A-A' is that the symmetric flow on either side of the extension axis is visible. Here, vectors indicate lower crustal

flow towards the Colorado Plateau. The Colorado Plateau itself continues to exhibit low velocity magnitudes. In the Rio Grande Rift crustal flow primarily occurs in the lower crust with a strong subsidence signal (Figure 11A)

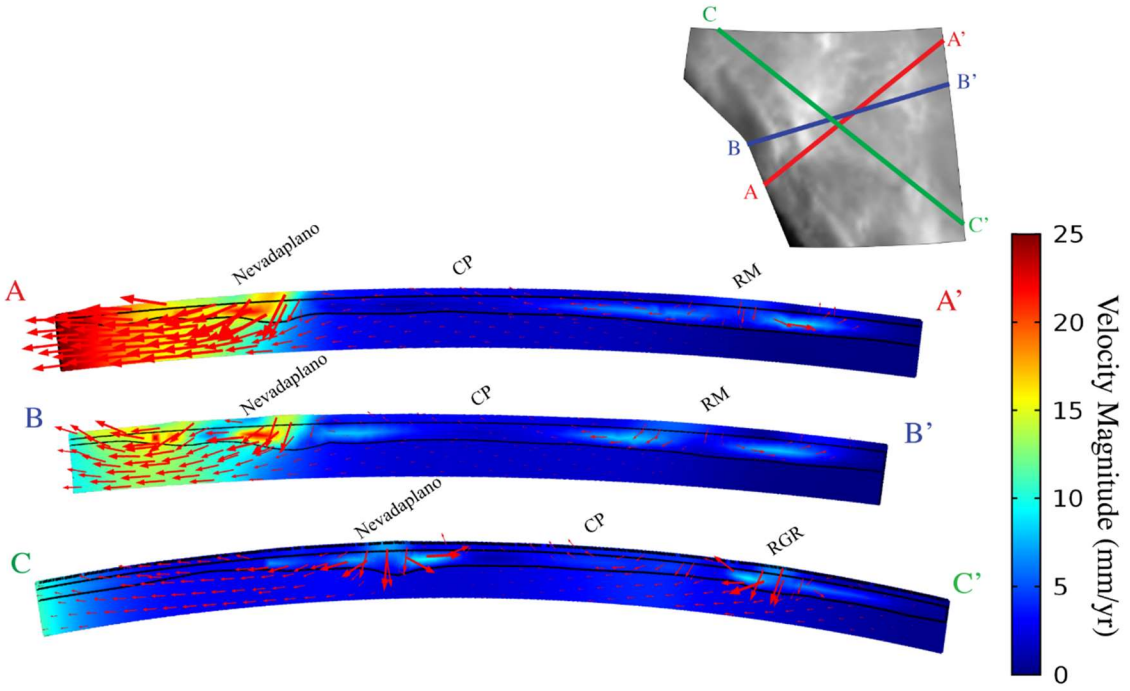

Figure 12: Cross sections through the preferred model. Vector direction is denoted by the red arrows and magnitude is indicated by the color bar. CP is the Colorado Plateau and RGR is the Rio Grande Rift. Important to note that arrows are not to the same scale on each cross section, refer to the colorbar for magnitude.

CHAPTER 4. DISCUSSION AND CONCLUSIONS

Computational modeling is a useful tool for simulating the physical processes that lead to different deformational driving forces, but often these solutions are non-unique. Our particular modeling framework also neglects the importance of elastic deformation on short time scales and our partitioning of viscosity may not reflect the actual conditions of the Earth at 17 Ma. Taking these limitations into consideration we can vary viscosity parameters and utilize observed geologic data to produce robust inferences into the driving forces and their relative contribution to the extension and formation of the Basin and Range, metamorphic core complexes and the Rio Grande rift.

Our suite of models with varying viscosity structures identifies the relative contribution of plate boundary forces and gravitational potential energy on Basin and Range extension. The comparison of our preferred model and the fixed boundary condition case emphasizes the importance of gravitational potential energy and a weak, thick lower crust under high topography. Our models also reveal that gravitational potential energy plays an important role in metamorphic core complex formation and Rio Grande Rift extension and the rotation of the Colorado Plateau.

4.1 Driving forces of Basin and Range extension

The forces that drive Basin and Range extension have long been debated (Flesch et al., 2000, 2007; Ghosh and Holt, 2012; Humphreys and Coblentz, 2007; Sonder and Jones, 1999). Boundary conditions, gravitational potential energy, and basal tractions are all competing forces that drive extension. Though modern Basin and Range mechanics are relatively well understood, previous work has not been able to discern the relative importance of each mechanism or create a spatially consistent model result that accounts for past deformation over the evolution of the Basin and Range, Colorado Plateau, and Rio Grande Rift.

Previous studies have reconstructed boundary conditions, topography and crustal thicknesses, density, and average vertical velocities for the western U.S (McQuarrie and Wernicke, 2005; Bahadori et al., 2018, Bahadori and Holt 2019). Despite these striking advances in

understanding the deformational history of the western U.S. and Basin and Range, numerical models have not been able to reproduce deformation that is consistent with geologic observations and signals across the Nevadaplano, Colorado Plateau, and Rio Grande rift. Our contribution is to use the previous reconstructed data in 3D and produce a partitioned 3D viscosity structure for the Basin and Range that produces consistent results with geologic observations and deformational signals across the region.

Before determining the relative impact of gravitational potential energy and boundary conditions, we must determine a 3D viscosity structure for the western U.S. Lateral variations of viscosity in the Basin and Range lithosphere are well understood, however, the vertical distribution of lithospheric strength remains contested (Burov & Watts, 2006; Jackson, 2002). Previous studies have reconstructed effective vertical average viscosities (Bahadori and Holt, 2019), but have not been able to determine the 3D distribution of strength within the lithosphere. By comparing the predicted surface velocities and vertical velocities of differing 3D viscosity structures with reconstructed surface velocities and fluorite deposit locations we determine that the best fit viscosity structure for the western U.S. fits with a "crème brûlée" model framework. Here, the upper crust has 5 times the strength of the lithospheric mantle (FCM 5) and the lithospheric mantle viscosity differs slightly with a weaker lower crust that has a viscosity of $10^{20.3}$ Pa-s.

To understand the relative importance of boundary conditions and gravitational potential energy during rifting we create a model case with active plate boundary conditions from a reconstruction from Bahadori and Holt. (2019) and a model case with fixed boundary conditions, allowing the only acting force to be gravity. When comparing these two model cases (Figure 10, 11) we see the vector orientations nearly match and provide a good fit with the metamorphic core complex vergence directions. This is also evident in the vertical velocity signals for both cases. Maximum subsidence rates for the fixed boundary case are only slightly higher than the preferred model. Additionally, outside of the Nevadaplano, deformation signals in the horizontal upper and lower crustal velocities are nearly identical between the two cases. This indicates that gravitational potential energy is the main contributor to deformation in the basin and range and the plate boundary conditions serve to rotate the vectors near the plate boundary, which is different from the nearly equal contribution observed in the western US today.

4.2 Implications for metamorphic core complex formation

Extension of high magnitudes produces regions of exposed deep crustal metamorphic rocks called metamorphic core complexes (Davis et al. 1980). During extensional processes, as the crust thins, deep crustal strata are exhumed from beneath an area of detachment and are exposed at the surface (Davis et al, 1980; Wernicke and Axen, 1988). Metamorphic core complexes are characterized by a core of high-grade metamorphic rocks and a cap of highly sheared, attenuated, and variably metamorphosed sedimentary rock. The formation of these structures remains controversial. Mechanisms include: extension on low angle normal faults (Wernicke, 1981), intrusions of plutons (Lister and Baldwin, 1993), the rotation of high angle normal faults (Buck, 1988), and the extrusion of a weak lower crust (Block and Royden, 1990; Bird, 1991; Martinez et al., 2001).

Our best fit model can inform the formation of metamorphic core complexes in the Basin and Range. Our results support the hypothesis that metamorphic core complexes are the result of flow in the lower crust. To further examine the lower crustal flow in 3D we produce cross-sections through the best fit model (Figure 12) and plot differential velocity (Figure 13). A-A' and B-B' (Figure 12) show a southwest-northeast cross-section along strike with metamorphic core complex vergence offering a 3D view into the lithosphere scale deformation occurring there. Under the Nevadaplano we see a high velocity zone of flow in the lower crust; this lateral extrusion of the lower crust serves as a mechanism for both core complex formation and the flattening of the Moho that is observed at present day. The differential velocities (Figure 13) show that regions where lower crust is flowing faster than the upper crust are co-located with core complexes. Though regions of highest differential velocity are not associated with known core complexes at this time period, it is likely these core complexes are not exposed at the surface. Our best fit model predicts differential velocities of 1-5 mm/yr and displacements of 3-15 km over the lifetime of the core complexes. Additionally, because the model predicted lower crustal velocity field provides a nearly identical match to the measured core complex vergence directions we believe that these vergence directions are actually recording the extrusion or flow of the lower crust during core complex formation (Block and Royden, 1990; Bird, 1991; McKenzie and Jackson, 2002). This also suggests that the primary driving force for their formation in the Nevadaplano is gravitational collapse.

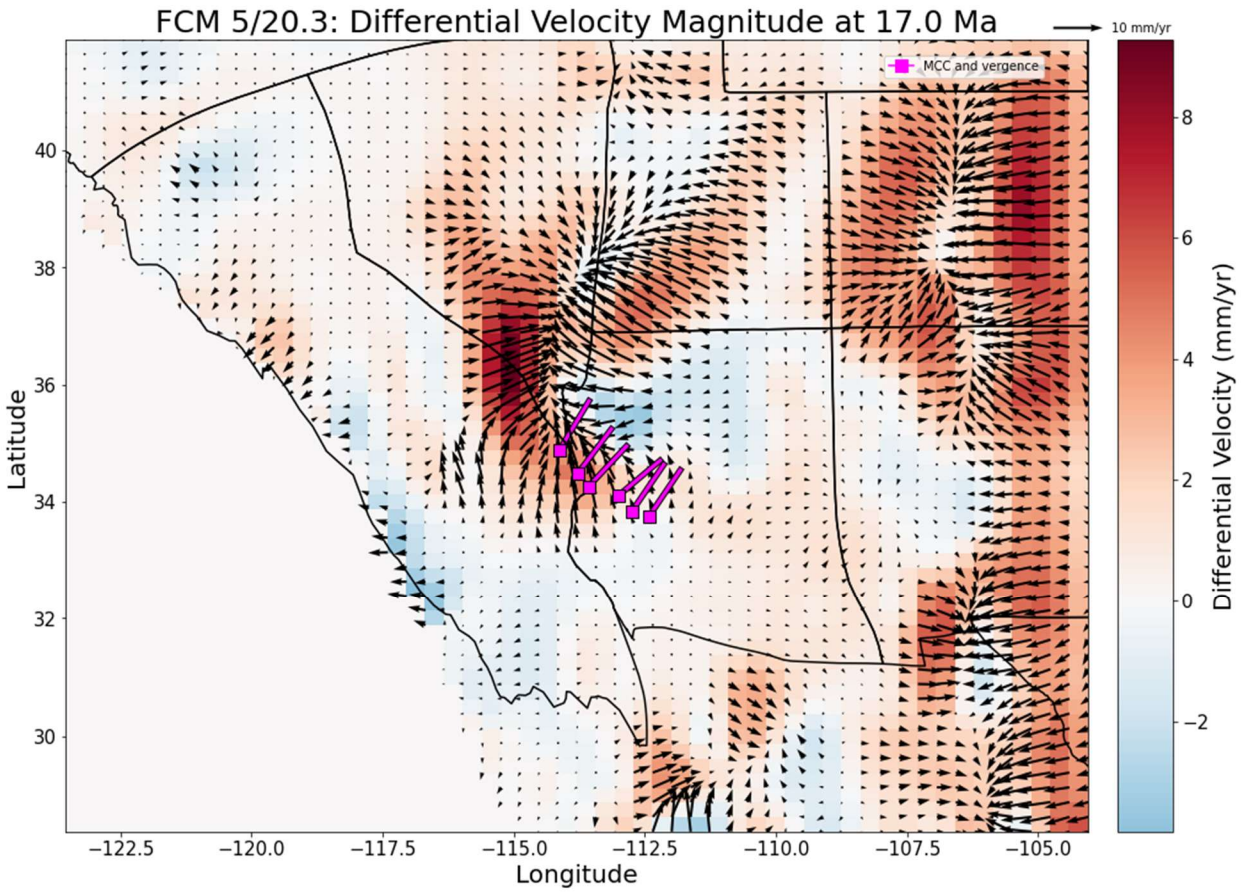

Figure 13: The differential flow of the best fit model, where differential flow is the surface velocity minus the lower crustal velocity (black arrows and colorbar). Deeper red colors indicate the lower crust is moving faster than the upper crust. Metamorphic core complex locations and vergence are indicated by magenta squares with tick marks.

4.3 Implications for the Colorado Plateau and the formation of the Rio Grande Rift

While the Basin and Range and Rio Grande rift underwent extension during 17 Ma, the Colorado Plateau experienced a period of uplift and tilting without undergoing significant internal deformation (Roberts et al., 2012; Davis et al., 2009). Most agree that tectonic mechanisms that produces horizontal plate motions cannot fully explain this uplift. As such, suggested uplift mechanisms for the Colorado Plateau are lateral crustal flow from adjacent thickened (McQuarrie and Chase, 2000), partial lithospheric mantle removal (Bird, 1979), increased heat flux from extension (Roy et al, 2009), and dynamic support from mantle upwelling (Parsons and McCarthy, 1995). Despite undergoing little internal deformation, the Colorado Plateau plays a role in the formation of the Rio Grande rift. Previous studies have linked a rotation of 1.0-1.5 degrees of the Colorado Plateau about a Euler pole near the Utah-Wyoming border to the extensional behavior of the Rio Grande Rift (Chapin and Cather, 1994). The Rio Grande Rift has undergone 8-12% extension in the North and up to 50% in the southern portion on the rift (Chapin and Cather, 1994; Aldrich et al., 1986; Morgan et al., 1986). Though many 2D models of Rio Grande rift formation exist (Wilson et al, 2005; Van Wijk et al., 2008) none have implemented a comprehensive regional 3D geometry with laterally and vertically varying viscosity structures that include deformation in the Basin and Range as well as the Colorado Plateau. Our contribution is to implement a consistent 3D model that includes the deformational signatures from the Basin and Range with a 3D partitioned viscosity structure to define the formation of the Rio Grande rift.

Our best fit model provides possible support for the rotation of the Colorado Plateau (Figure 10). The influx of lower crustal flow along the flanks of the Colorado Plateau may generate enough motion to accommodate the very small rotations put forward by Chapin and Cather (1994). This lateral flux of lower crustal flow (Roberts et al., 2012; Davis et al., 2009; McQuarrie and Chase, 2000) is also likely responsible for the tilt and uplift of the Colorado Plateau expressed in the vertical velocity signature that is observed here (Figure 11A) and in river profile studies (McQuarrie and Chase, 2000; Roberts et al., 2012). When looking at surface velocities (Figure 11A) and in 3D (Figure 12, C-C') we clearly observe the Northwest-Southeast tilt of the Colorado Plateau expressed in vertical velocity components and the largest velocity magnitudes located in the lower crust of the Rio Grande rift. This suggests that lower crustal flow also facilitates extension in the Rio Grande rift in tandem with the rotation of the Colorado Plateau.

4.4 Conclusions

We develop three-dimensional, lithospheric scale models that incorporate laterally and vertically varying density and viscosity with reconstructed boundary conditions to investigate the effect of a weak lower crust on Basin and Range extension history and the relative contributions of forces acting on the Basin and Range. We determined a best fit 3D viscosity structure including a weak lower crust with a viscosity of $10^{20.3}$ Pa-s and with a FCM of 5 to partition the upper crustal and lithospheric mantle strength. Our results suggest the following:

1. The primary driving force of the formation of geologic features in the western US is regional gravitational collapse focused in the lower crust. Plate motions are second order by comparison at this time period and act to rotate velocities near the plate boundary.

2. A weak lower crust is a prerequisite for metamorphic core complex formation and extension in the Nevadaplano. Lateral extrusion of the lower crust serves as a mechanism for both core complex formation and the flattening of the Moho that is observed at present day.

3. Lower crustal motion is a contributing driving force for the rotation and tilt of the Colorado Plateau and formation of the Rio Grande Rift.

REFERENCES

Aldrich, M. J., Chapin, C. E., & Laughlin, A. W. (1986). Stress history and tectonic development of the Rio Grande rift, New Mexico. Journal of Geophysical Research: Solid Earth, 91(B6), 6199-6211.

Bahadori, A., & Holt, W. E. (2019). Geodynamic evolution of southwestern North America since the Late Eocene. Nature communications, 10(1), 1-18.

Bahadori, A., Holt, W. E., & Rasbury, E. T. (2018). Reconstruction modeling of crustal thickness and paleotopography of western North America since 36 Ma. Geosphere, 14(3), 1207-1231.

Bird, P. (1991). Lateral extrusion of lower crust from under high topography in the isostatic limit. Journal of Geophysical Research: Solid Earth, 96(B6), 10275-10286.

Bird, P. (1979). Continental delamination and the Colorado Plateau. Journal of Geophysical Research: Solid Earth, 84(B13), 7561-7571.

Bischoff, S., & Flesch, L. (2019). Impact of lithospheric strength distribution on India-Eurasia deformation from 3-D geodynamic models. Journal of Geophysical Research: Solid Earth, 124(1), 1084-1105.

Bischoff, S. H., & Flesch, L. M. (2018). Normal faulting and viscous buckling in the Tibetan Plateau induced by a weak lower crust. Nature communications, 9(1), 1-9.

Buck, W. R. (1988). Flexural rotation of normal faults. Tectonics, 7(5), 959-973.

Burov, E. B., & Watts, A. B. (2006). The long-term strength of continental lithosphere:" jelly sandwich" or" crème brûlée"?. GSA today, 16(1), 4.

Chapin, C. E., Cather, S. M., & Keller, G. R. (1994). Tectonic setting of the axial basins of the northern and central Rio Grande rift. Special Papers-Geological Society of America, 5-5.

Chen, W. P., & Molnar, P. (1983). Focal depths of intracontinental and intraplate earthquakes and their implications for the thermal and mechanical properties of the lithosphere. Journal of Geophysical Research: Solid Earth, 88(B5), 4183-4214.

Coney, P. J. (1980). Cordilleran metamorphic core complexes: An overview. Cordilleran metamorphic core complexes: Geological Society of America Memoir, 153, 7-31.

Coney, P. J., & Harms, T. A. (1984). Cordilleran metamorphic core complexes: Cenozoic extensional relics of Mesozoic compression. Geology, 12(9), 550-554.

Davis, G. H., Bump, A. P., Kay, S. M., Ramos, V. A., & Dickinson, W. R. (2009). Structural geologic evolution of the Colorado Plateau (pp. 99-124). Geological Society of America.

Dickinson, W. R. (2002). The Basin and Range Province as a composite extensional domain. International Geology Review, 44(1), 1-38.

Flesch, L. M., Holt, W. E., Haines, A. J., & Shen-Tu, B. (2000). Dynamics of the Pacific-North American plate boundary in the western United States. Science, 287(5454), 834-836.

Flesch, L. M., Holt, W. E., Haines, A. J., Wen, L., & Shen-Tu, B. (2007). The dynamics of western North America: Stress magnitudes and the relative role of gravitational potential energy, plate interaction at the boundary and basal tractions. Geophysical Journal International, 169(3), 866-896.

Ghosh, A., & Holt, W. E. (2012). Plate motions and stresses from global dynamic models. Science, 335(6070), 838-843.

Holt, W. E., Chamot-Rooke, N., Le Pichon, X., Haines, A. J., Shen-Tu, B., & Ren, J. (2000). Velocity field in Asia inferred from Quaternary fault slip rates and Global Positioning System observations. Journal of Geophysical Research: Solid Earth, *105*(B8), 19185-19209.

Humphreys, E. D., & Coblentz, D. D. (2007). North American dynamics and western US tectonics. Reviews of Geophysics, 45(3).

Jackson, J. A. (2002). Strength of the continental lithosphere: time to abandon the jelly sandwich?. GSA today, 12, 4-10.

Kohlstedt, D. L., Evans, B., & Mackwell, S. J. (1995). Strength of the lithosphere: Constraints imposed by laboratory experiments. Journal of Geophysical Research: Solid Earth, 100(B9), 17587-17602.

Lamarre, A. L., & Hodder, R. W. (1978). Distribution and genesis of fluorite deposits in the western United States and their significance to metallogeny. Geology, 6(4), 236-238.

Lister, G. S., & Baldwin, S. L. (1993). Plutonism and the origin of metamorphic core complexes. Geology, 21(7), 607-610.

Martinez, F., Goodliffe, A. M., & Taylor, B. (2001). Metamorphic core complex formation by density inversion and lower-crust extrusion. Nature, 411(6840), 930-934.

McQuarrie, N., & Chase, C. G. (2000). Raising the Colorado Plateau. Geology, 28(1), 91-94.

McQuarrie, N., & Wernicke, B. P. (2005). An animated tectonic reconstruction of southwestern North America since 36 Ma. Geosphere, 1(3), 147-172.

Morgan, P., Seager, W. R., & Golombek, M. P. (1986). Cenozoic thermal, mechanical and tectonic evolution of the Rio Grande rift. Journal of Geophysical Research: Solid Earth, 91(B6), 6263-6276.

Parsons, T., & McCarthy, J. (1995). The active southwest margin of the Colorado Plateau: Uplift of mantle origin. Geological Society of America Bulletin, 107(2), 139-147.

Roberts, G. G., White, N. J., Martin-Brandis, G. L., & Crosby, A. G. (2012). An uplift history of the Colorado Plateau and its surroundings from inverse modeling of longitudinal river profiles. Tectonics, 31(4).

Roy, M., Jordan, T. H., & Pederson, J. (2009). Colorado Plateau magmatism and uplift by warming of heterogeneous lithosphere. Nature, 459(7249), 978-982.

Sonder, L. J., & Jones, C. H. (1999). Western United States extension: How the west was widened. Annual Review of Earth and Planetary Sciences, 27(1), 417-462.

Van Wijk, J., Van Hunen, J., & Goes, S. (2008). Small-scale convection during continental rifting: Evidence from the Rio Grande rift. Geology, 36(7), 575-578.

Wernicke, B., Burchfiel, B. C., Lipman, P. W., & Zoback, M. L. (1992). Cenozoic extensional tectonics of the US Cordillera. The Geology of North America, 3, 553-581.

Wernicke, B. (1981). Low-angle normal faults in the Basin and Range Province: nappe tectonics in an extending orogen. Nature, 291(5817), 645-648.

Wilson, D., Aster, R., West, M., Ni, J., Grand, S., Gao, W., ... & Patel, P. (2005). Lithospheric structure of the Rio Grande rift. Nature, 433(7028), 851-855.

Zuber, M. T., Parmentier, E. M., & Fletcher, R. C. (1986). Extension of continental lithosphere: a model for two scales of Basin and Range deformation. Journal of Geophysical Research: Solid Earth, 91(B5), 4826-4838.

VITA

Education

Purdue University
August 2015-Present
B.S. Geology and Geophysics (2019)
M.S. Geophysics
Advisor: Lucy Flesch
Thesis: Investigating the effect of a weak lower crust on Basin and Range extension history

Experience

Teaching Assistantships:

- *2018 Fall:* Taught a lab portion of EAPS 112: Earth Through Time and held review sessions for exam material.
- *2018 Spring:* Assisted with EAPS 116: Earthquakes and Volcanoes (online class) demonstrations and course work.

Service and Public Outreach

Service:

- EAPS Graduate Student Association President 2020-21
- Department Graduate Committee Member student member 2020-21t
- Department Strategic Planning Committee student member 2020-21
- Purdue University Geological Society Web Coordinator 2017-2019

Talks/Public Outreach:

- Plate Tectonics, Volcanoes, and Higher Education (9/13/19): Invited to present Earth science topics to the students of Angola Middle School.
- EAPS Passport day seismology booth: teaches elementary age students the basics of seismic waves.

Miscellaneous:

- Created "Basics of Julia and GMT" tutorial for the Geophysics Lab group.

Professional and Scholarly Associations

Association of Environmental and Engineering Geologists, student member
American Geophysical Union, student member

Awards and Honors

2021	Michael C. Gardner Memorial Award
2021	Mobil Oil Geology Award
2021	Terry R. West Award
2020	William J. Hinze Award
2018-2019	EAPS Class of 1970 Scholarship
2018	Teaching Honor Roll
2017-2021	Cedric J. Newby Award
2017-2018	Ned M Smith Field Camp Award
2017-2018	Purdue General Scholarship

2015-19 Marquis Renewable Scholarship

Certifications

Purdue University World Wise Multicultural Communications certificate
Purdue University Safe Zone certificate

Publications/Abstracts

Submitted:

1. Alireza Bahadori, William E. Holt, Tristan Salles, Louis Moresi, Romain Beucher, Neng Lu, Lucy M. Flesch, **Christopher Calvelage**, Ran Feng, Katharine M. Loughney, E. Troy Rasbury, Andre R. Potochnik, W. Bruce Ward, Kevin Hatton, Daniel M. Davis, Saad S. B. Haq Tara M. Smiley, Catherine Badgley. Lithosphere dynamics drive uplift of the Colorado Plateau and formation of the Grand Canyon. (Submitted for review).

Abstracts:

1. Bahadori, A., Holt, W. E., Flesch, L. M., & **Calvelage, C.** (2019). From Highlands to Basin and Range Province: the role of lithospheric geodynamic evolution in southwestern North America since Late Eocene. *AGUFM*, *2019*, T43E-0477.

2. **Calvelage, C.,** Flesch, L. M., Bahadori, A., & Holt, W. E. (2020). Investigating the effect of a weak lower crust on Basin and Range extension history. *AGUFM, 2020,* T034-0007